Cancer Research

Synergistic Enhancement of Carboplatin Efficacy with Photodynamic Therapy in a Three-Dimensional Model for Micrometastatic Ovarian Cancer

Imran Rizvi[1,3], Jonathan P. Celli[1], Conor L. Evans[1], Adnan O. Abu-Yousif[1], Alona Muzikansky[2], Brian W. Pogue[3], Dianne Finkelstein[2], and Tayyaba Hasan[1]

Abstract

Metastatic ovarian cancer (OvCa) frequently recurs due to chemoresistance, highlighting the need for non-overlapping combination therapies that mechanistically synergize to eradicate residual disease. Photodynamic therapy (PDT), a photochemistry-based cytotoxic modality, sensitizes ovarian tumors to platinum agents and biologics and has shown clinical promise against ovarian carcinomatosis. We introduce a three-dimensional (3D) model representing adherent ovarian micrometastases and high-throughput quantitative imaging methods to rapidly screen the order-dependent effects of combining benzoporphyrin-derivative (BPD) monoacid A–based PDT with low-dose carboplatin. 3D ovarian micronodules grown on Matrigel were subjected to BPD-PDT either before or after carboplatin treatment. We developed custom fluorescence image analysis routines to quantify residual tumor volume and viability. Carboplatin alone did not eradicate ovarian micrometastases at a dose of 400 mg/m^2, leaving surviving cores that were nonsensitive or impermeable to chemotherapy. BPD-PDT (1.25 μmol/L·J/cm^2) created punctate cytotoxic regions within tumors and disrupted micronodular structure. Treatment with BPD-PDT prior to low-dose carboplatin (40 mg/m^2) produced a significant synergistic reduction [$P < 0.0001$, analysis of covariance (ANCOVA)] in residual tumor volume [0.26; 95% confidence interval (95% CI), 0.19–0.36] compared with PDT alone (0.76; 95% CI, 0.63–0.92) or carboplatin alone (0.95; 95% CI, 0.83–1.09), relative to controls. This synergism was not observed with the reverse treatment order. Here, we demonstrate for the first time the use of a 3D model for micrometastatic OvCa as a rapid and quantitative reporter to optimize sequence and dosing regimens of clinically relevant combination strategies. This approach combining biological modeling with high-content imaging provides a platform to rapidly screen therapeutic strategies for a broad array of metastatic tumors. *Cancer Res; 70(22); 9319–28. ©2010 AACR.*

Introduction

The vast majority of ovarian cancer (OvCa) cases are diagnosed once the disease has metastasized to distant sites, which substantially diminishes the possibility of providing curative treatments (1–4). Despite advancements in surgical debulking techniques, optimization of chemotherapeutic regimens, and improvements in radiotherapy, 5-year progression-free survival (PFS) and overall survival (OS) rates remain low even among women whose disease is optimally cytoreduced to ≤1 cm in diameter (1, 5). These results indicate that unresected tumor nodules respond poorly to traditional agents, primarily due to poor drug penetration (6, 7) and the development of resistance (8–10). There is a critical need to design and rapidly evaluate more effective management strategies for residual OvCa. Identifying the most promising treatments among the vast library of candidate agents has been a slow and unreliable process due, in part, to a lack of high-throughput model systems that capture critical aspects of tumor biology (1, 11, 12). We address this limitation, by developing an *in vitro* three-dimensional (3D) model for adherent micrometastatic OvCa, which, in conjunction with custom image analysis routines designed in our group, serves as a high-throughput reporter for treatment efficacy. We use this platform to evaluate a mechanism-based combination regimen that synergistically enhances carboplatin efficacy with photodynamic therapy (PDT), a photophysical cytotoxic modality that sensitizes OvCa cells to chemo and biological agents (4, 13), and has shown promise in clinical trials for the treatment of ovarian carcinomatosis (14–19).

Authors' Affiliations: [1]Wellman Center for Photomedicine, Massachusetts General Hospital, Harvard Medical School; [2]Biostatistics Center, Massachusetts General Hospital, Boston, Massachusetts and [3]Thayer School of Engineering, Dartmouth College, Hanover, New Hampshire

Note: Supplementary data for this article are available at Cancer Research Online (http://cancerres.aacrjournals.org/).

Corresponding Author: Tayyaba Hasan, Wellman Center for Photomedicine, Massachusetts General Hospital, 40 Blossom Street, Boston, MA 02114. Phone: 617-726-6996; Fax: 617-726-8566; E-mail: thasan@partners.org.

doi: 10.1158/0008-5472.CAN-10-1783

Rationally designed combination therapies provide the best hope of improving outcomes for patients with advanced stage disease, by exploiting nonoverlapping cellular targets, improving drug transport, and mitigating the survival signals that lead to treatment resistance (1, 4, 8, 13, 20–22). Despite improvements from combining chemotherapeutics (2, 9, 10, 23), rates of recurrence in patients with advanced stage OvCa remain as high as 80%, indicating that traditional chemotherapies by themselves hold little promise of significantly effecting PFS and OS (8, 9).

We (4, 13) and others (21, 22) have shown that PDT-based combination regimens sensitize tumors, including OvCa, to chemotherapeutics and targeted biological inhibitors. PDT involves activation of a photosensitive molecule by light of a specific wavelength to generate reactive species (18, 21, 24–29) and is approved for a variety of applications including actinic keratosis, non–small cell lung cancer, and palliation of obstructive esophageal cancer using Photofrin (24, 26). PDT is also approved globally as a first line therapy for age-related macular degeneration (24) using benzoporphyrin-derivative monoacid ring A (BPD-MA; verteporfin), which offers better photobiological activity and shorter cutaneous phototoxicity than Photofrin (4, 29–31).

BPD also provides promising results for the treatment of multifocal OvCa (4, 31, 32). We have reported that BPD-PDT combined with Erbitux, an antibody that targets the epidermal growth factor receptor, synergistically reduces tumor burden and enhances survival in a mouse model for ovarian carcinomatosis (4). Combining these mechanistically distinct monotherapies mitigates the limitations of each modality (4). Molpus and colleagues showed that multiple cycles of BPD-PDT were required to achieve a therapeutic benefit in a murine model for ovarian carcinomatosis (31). Erbitux, a cytostatic therapy, is administered at high doses for extended periods with modest improvements in survival (33). Combining BPD-PDT with Erbitux improved acute and long-term therapeutic outcomes, with fewer treatment cycles and minimal toxicity (4). These promising results have informed large animal studies leading to clinical trials using BPD-PDT in combination with Erbitux to treat metastatic OvCa (32, 34).

In a variant of this approach, photoimmunotherapy (PIT), chlorin e_6 was conjugated to a monoclonal antibody, OC125, creating a therapeutically active targeting moiety (13). In cisplatin-resistant tissue, PIT reversed chemoresistance and produced a synergistic 12.9-fold increase in cytotoxicity compared with cisplatin alone. The combination treatment had an additive effect in cisplatin-sensitive tissue. Among all patient tissue samples and cell lines, PIT increased OvCa sensitivity to cisplatin by 6.9-fold compared with cisplatin alone (13).

Here, we introduce an *in vitro* 3D tumor model for adherent, micrometastatic OvCa, adapted from breast cancer models (35, 36), as a treatment response platform to efficiently evaluate combination therapies. These ovarian 3D tumors represent unresectable, multifocal micronodules that are typically managed with chemotherapy and are precursors to recurrent metastatic disease (1–3). We use this biological and imaging-based platform to determine the effect of combining BPD-PDT and carboplatin. We hypothesized that the interaction between these mechanistically distinct cytotoxic modalities would lead to synergistic enhancement of the monotherapies. Our results show that carboplatin alone does not eradicate OvCa at clinically relevant doses and demonstrate for the first time a sequence-dependent synergistic enhancement of carboplatin efficacy by BPD-PDT.

Materials and Methods

Cell lines and culture

NIH:OVCAR5 human epithelial OvCa cells were obtained from Thomas Hamilton (Fox Chase Cancer Institute) and previously characterized by microsatellite marker analysis. Cells were maintained as previously described (4).

Monolayer cultures. OVCAR5 cells were plated in 35-mm dishes (BD Biosciences) at a density of 210,000 in 2 mL medium.

3D cultures. Protocols for 3D ovarian cultures were adapted from previously published methods for breast cancer cell lines (35, 36). Briefly, 150 or 250 μL growth factor reduced-Matrigel (GFR-Matrigel; BD Biosciences) was pipetted into the center well of a chilled 35-mm MatTek dish (P35G-0-20-C; MatTek Corp.) or each well of a black-walled 24-well plate (Genetix W1350). An OVCAR5 single cell suspension (500 μL of 1.5×10^4 cells/mL) was pipetted onto each dish/well. After 30 minutes, 3D culture medium was added to a final concentration of 2% GFR-Matrigel and changed every 2 to 3 days.

Growth characterization

Darkfield microscopy images (five fields per culture per time point) were acquired using an inverted microscope (Zeiss Axiovert 100 TV) with a charge-coupled device camera (Quantifire XI) and saved as uncompressed TIFFs. Image data were batch-processed using custom MATLAB (Mathworks) routines to report equivalent diameters of automatically segmented (nearly) circular regions corresponding to 3D nodules as previously described (37). *N* values represent individual 3D culture dishes, and SDs report the reproducibility of mean diameter from independent platings. Time lapse of 10× phase contrast sequences were obtained using a Nikon TE2000-S microscope in a weather station (37°C, 5% CO_2).

Immunofluorescence protocol

A previously established immunofluorescence protocol was used (38). Human fibronectin (Sigma F0916) and mouse anti-E-cadherin (Transduction Laboratories C20820) antibodies were fluorescently labeled using Alexa $Fluor_{568}$ goat anti-mouse secondary antibodies (A11004, Invitrogen). 4′,6-Diamidino-2-phenylindole (DAPI; Sigma 32670) was diluted 1:1,000 in PBS to stain nuclei.

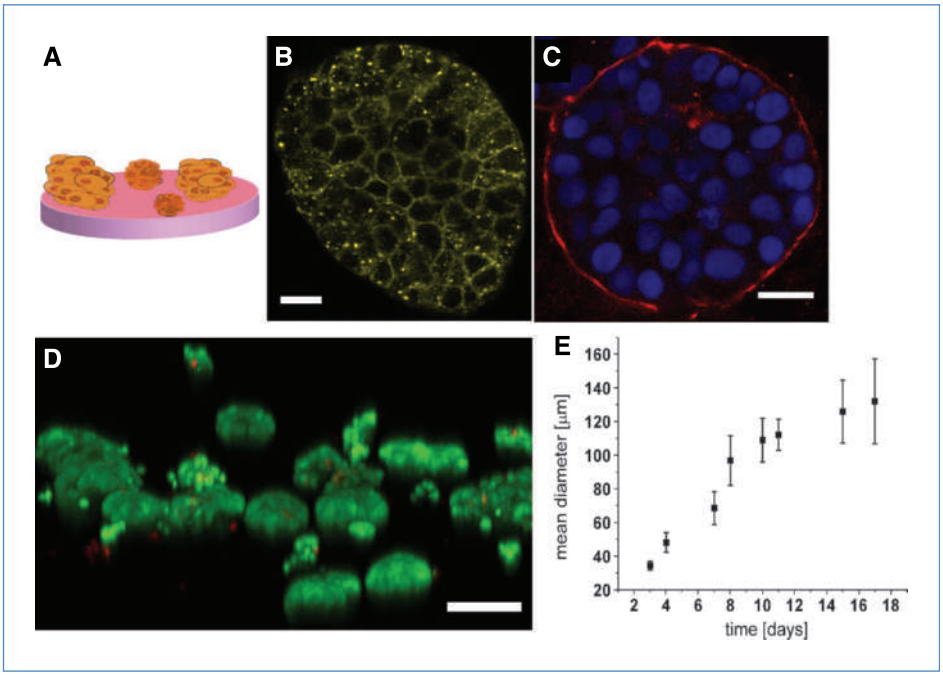

Figure 1. Biological characterization of a 3D model for micrometastatic OvCa. A, OVCAR5 cells overlaid on GFR-Matrigel formed 3D ovarian micronodules representing adherent micrometastatic disease with punctate E-cadherin expression (B) and fibronectin (red) expression (blue, DAPI; C) markers for poor prognosis. D, mean diameter increased from 34.3 μm (±2.6 μm) 3 d postplating (n = 9) to 108.9 μm (±13.0 μm) at day 10 (n = 9) and 131.9 μm (±25.3 μm) at day 17 (n = 3; E). Scale bars, 20 μm (B and C) and 150 μm (D).

Treatments

Carboplatin. To establish dose response in monolayer versus 3D, cultures were treated with 0.4–400 mg/m^2 carboplatin in either standard medium (monolayer) or standard medium with 2% GFR-Matrigel (3D medium). Cytotoxicity was evaluated following either a 24-hour incubation in monolayer or 96-hour incubation in 3D cultures. Carboplatin treatments for all combination therapy experiments were initiated on day 10 postplating and terminated on day 14 using a dose of 40 mg/m^2 to keep the carboplatin dose and incubation period fixed for both treatment sequences.

PDT. Cultures were incubated with 250 nmol/L BPD-MA (QLT, Inc.) for 90 minutes in standard medium. Immediately prior to irradiation, BPD-MA medium was replaced with either fresh standard medium (monolayer cultures) or standard medium with 2% GFR-Matrigel (3D cultures). Each dish/well was irradiated with a 690-nm fiber-coupled diode laser (Model 7401; High Power Devices, Inc.) at a fluence rate of 40 mW/cm^2 (VEGA Laser Power Energy Meter, Ophir Laser Measurement Group, LLC). For monolayer versus 3D culture experiment, fluences of 0.1, 1.0, 2.5, or 5.0 J/cm^2 were delivered for total PDT doses ([PS] × fluence) of 0.025, 0.25, 0.625, and 1.25 μmol/L·J/cm^2, respectively. To determine sequence-dependent cytotoxic response in combination therapy experiments, 3D cultures were treated with 1.25 μmol/L·J/cm^2 BPD-PDT on either day 10 or day 14 postplating (prior to or on completion of carboplatin treatment, respectively).

Controls were subjected to sham manipulations. N values for treatment studies represent individual 3D cultures over a minimum of three independent platings.

High-throughput fluorescence imaging and cytotoxicity analysis

Cultures were incubated with LIVE/DEAD reagents (Invitrogen, L-3224), calcein AM (live), and ethidium bromide (dead), which overcome limitations of MTT and MTS that bind to GFR-Matrigel. Using an Olympus FV-1000 confocal microscope with automated stage, multichannel fluorescence images from multiwell dishes were acquired in high throughput using a 4× objective (488 nm excitation, with FITC emission filter and 559 nm excitation, with TRITC emission filter for calcein and ethidium homodimer-1, respectively). Laser and photomultiplier tube settings, optimized for maximum dynamic range, were internally consistent across experimental groups.

Therapeutic efficacy was quantified by two metrics: (a) residual tumor volume, a measure of how much viable disease remains on each plate, and (b) tumor viability, a ratiometric quantification of how viable the residual disease is. Image data sets were batch-processed using custom MATLAB routines (37). Calcein images were segmented (as above) to calculate nodule volumes from equivalent diameters, d_{eq}, by,

$$v = \frac{3}{4}\pi\left(\frac{d_{eq}}{2}\right)^3$$

and then summed to determine total volume reported as fraction of the no-treatment control. Tumor viability was quantified by the ratio of calcein to total fluorescence intensity (calcein plus ethidium) and normalized to no treatment as previously described (37).

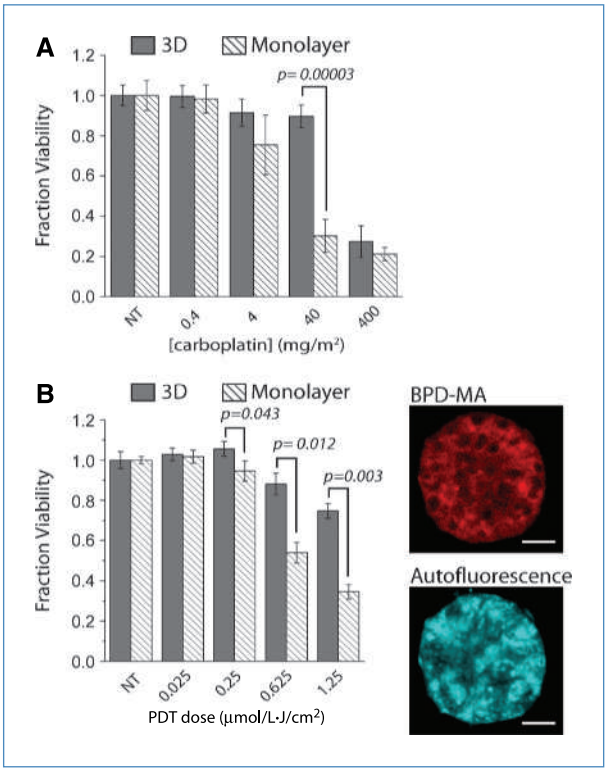

Figure 2. Monolayer cultures significantly overestimate carboplatin and BPD-PDT efficacy compared with cells in 3D. A, fractional viability of OVCAR5 cells in monolayer (striped) following carboplatin treatment (40 mg/m^2) was 0.30 (±0.082; n = 10) compared with 0.90 (±0.057) in 3D (solid; n = 6; P < 0.001, two-tailed t test). B, left, monolayer cultures treated with 1.25 μmol/L·J/cm^2 BPD-PDT had a fractional viability of 0.35 (±0.04; n = 12) compared with 0.75 (±0.04) in 3D (n = 13; P = 0.003, two-tailed t test). N values vary from 6 to 16 for individual treatment groups within each culture condition. B, right, confocal fluorescence images show BPD-MA distribution and autofluorescence from a representative nodule. Scale bars, 25 μm.

Statistical analysis

For each experiment, we fit ANCOVA models for the effect from each intervention (PDT, carboplatin, and the combination treatments), adjusting for batch and day (which ensured that the proper control group was used for the comparison). To keep the carboplatin dose and schedule fixed for both treatment sequences, the time points for PDT treatment and cytotoxic evaluation had to be adjusted between the two sequences as described in Treatments. Statistical analysis for synergism was conducted independently for each sequence, with separate and appropriate controls for each of the two combination treatment schedules. To analyze the synergy, we fit a single ANCOVA model with indicators for carboplatin and PDT, and the interaction between these variables was the basis for assessing the effect of the combination above that of the additive effects of each treatment alone. All analyses were performed on the log-transformed variables (of proportion viable and tumor volume), so the parameter associated with the difference of treatment versus control (from the ANCOVA) was then exponentiated to summarize the effect of treatment on each of these measures of outcome. As a result of this, the confidence intervals will not be symmetrical about the mean. Analyses were performed separately for each sequence.

Results

Model development and size characterization

OVCAR5 cells overlaid as a single-cell suspension on a bed of GFR-Matrigel spontaneously formed 3D multicellular tumor nodules resembling adherent micrometastatic disease (Fig. 1A–D). Ten days after plating, the 3D micronodules demonstrated cell surface and intracellular punctate E-cadherin expression (Fig. 1B), a distribution pattern associated with metastatic ovarian tumors (3, 39). Micronodules were also encapsulated in a basement membrane containing human fibronectin (Fig. 1C), a marker correlated with metastatic, chemoresistant, and recurrent disease, indicating the poorest outcome for OvCa patients (40, 41). Migration, assembly, and proliferation events (Supplementary Movie S1) led to heterogeneous 3D nodules resembling micrometastatic disease within 11 days of plating (Fig. 1D). The micronodules grew from a mean diameter of 34.3 μm (±2.6 μm) 3 days postplating (n = 9) to a mean diameter of 108.9 μm (±13.0 μm) at day 10 (n = 9) and 131.9 μm (±25.3 μm) at day 17 (n = 3; Fig. 1E).

Differential response to treatment with carboplatin and PDT in monolayer versus 3D

Cytotoxic response to escalating doses of carboplatin or PDT in 3D versus traditional monolayer cultures (Fig. 2A and B) was evaluated by quantitative imaging of LIVE/DEAD reagents. Monolayer cultures significantly overestimate the sensitivity of OvCa cells to carboplatin treatment. At 40.0 mg/m^2 (one tenth of the clinically effective dose for i.p. administered carboplatin; ref. 42) OVCAR5 cells showed 3-fold higher sensitivity to carboplatin in monolayer than the same cells in 3D: 0.30 (±0.082) fraction viability in monolayer (n = 10) compared with 0.90 (±0.057) fraction viability in 3D (n = 6; P < 0.001, two-tailed t test), relative to no treatment controls (n = 11 and 6 for monolayer and 3D, respectively; Fig. 2A).

At a PDT dose of 1.25 μmol/L·J/cm^2 (0.250 μmol/L BPD and 5.0 J/cm^2 of 690 nm light), the fraction viability in monolayer OVCAR5 cultures was 0.35 (±0.04; n = 12), relative to no treatment controls (n = 12; Fig. 2B). At the same PDT dose in 3D, the fraction viability was 0.75 (±0.04; n = 13), relative to no treatment controls (n = 16). These notable differences in viability indicate that OVCAR5 cells are more than twice as sensitive to BPD-PDT in monolayer compared with the same cells in 3D cultures (P = 0.003, two-tailed t test).

3D model reveals differential patterns of cytotoxic response for carboplatin versus PDT

Close examination of cytotoxicity in 3D ovarian micronodules treated 10 days after plating with either carboplatin or PDT alone revealed distinct cell death patterns for the individual monotherapies (Fig. 3A and B). A persistent

population of viable surviving cores was observed following incubation with 400 mg/m^2 carboplatin. As shown in a representative nodule (Fig. 3A), the ethidium bromide (dead) signal had a peak width of 15 to 20 μm (full width at half maximum) on the periphery of carboplatin-treated micronodules, which overlapped minimally with calcein green (live) fluorescence from the inner core of the same micronodule. This cytotoxicity pattern indicates the presence of a surviving core that was nonsensitive or impermeant to carboplatin.

Similar analysis of BPD-PDT–treated micronodules revealed a contrasting cytotoxic pattern. Figure 3B shows a representative micronodule treated with 1.25 μmol/L·J/cm^2 BPD-PDT and fluorescence intensity profiles from two regions of interest in the micronodule. BPD-PDT disrupts micronodular structure and creates punctuate regions of highly overlapping calcein green and ethidium bromide fluorescence peaks.

Sequence-dependent synergistic reduction in viability and tumor burden in 3D micronodules treated with combination PDT and carboplatin

Based on the distinct cytotoxic mechanisms for carboplatin (8, 23, 42) versus BPD-PDT (4, 27, 29) and the differential cell death patterns observed here, we hypothesized that the two modalities could synergize to enhance efficacy at lower doses. We tested this hypothesis by treating the ovarian

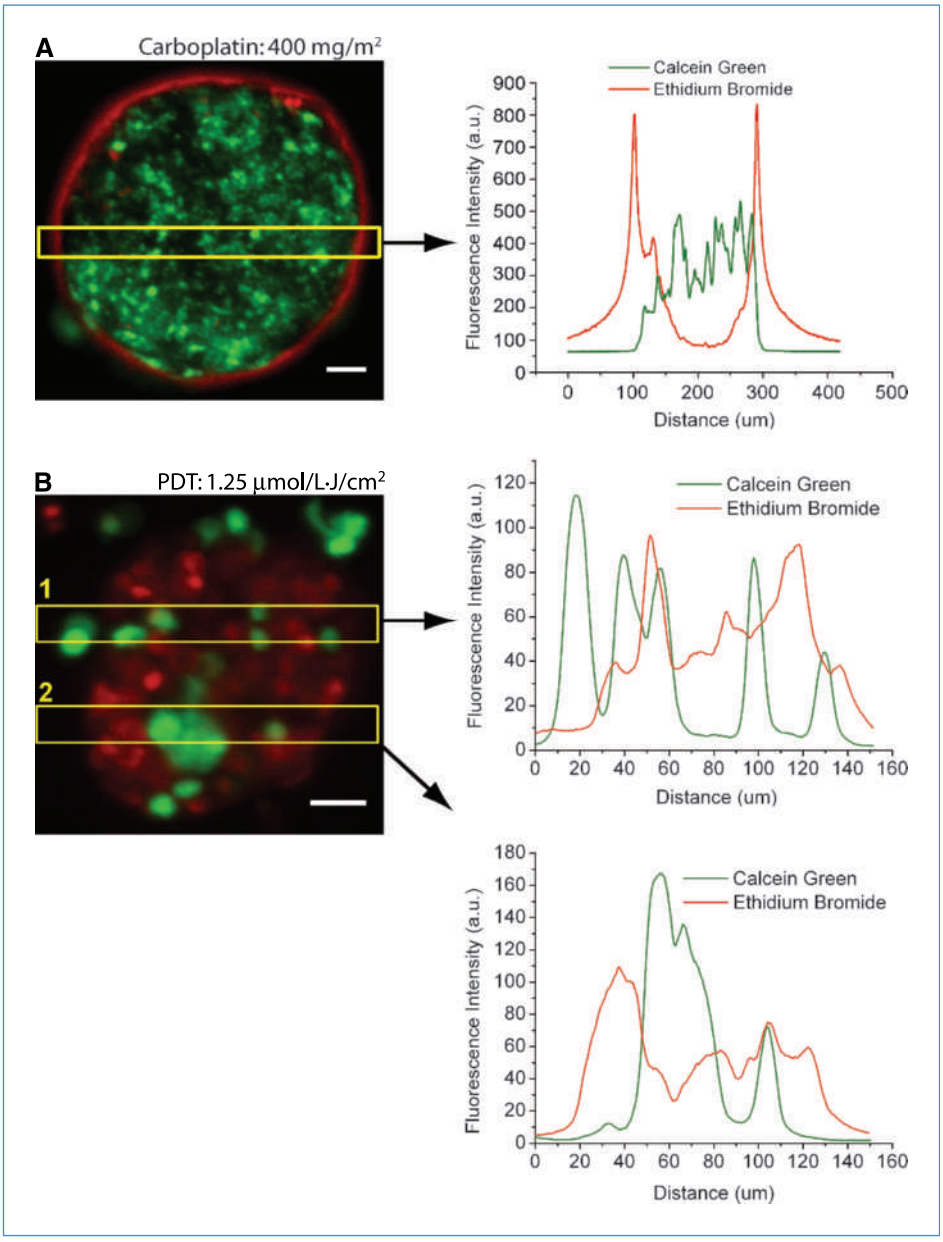

Figure 3. Differential patterns of cytotoxic response in carboplatin-treated and BPD-PDT–treated 3D micronodules. A, left, a representative micronodule treated with 400 mg/m^2 carboplatin showing cell death (ethidium bromide) on the periphery of a viable (calcein) tumor core, with distinct and minimally overlapping fluorescence intensity profiles (right). B, left, BPD-PDT 1.25 μmol/L·J/cm^2 treatment leads to nodular disruption and punctate cytoxicity. B, right, intensity profile scans through two regions of interest (yellow boxes) show highly overlapping fluorescence patterns. Scale bars, 25 μm.

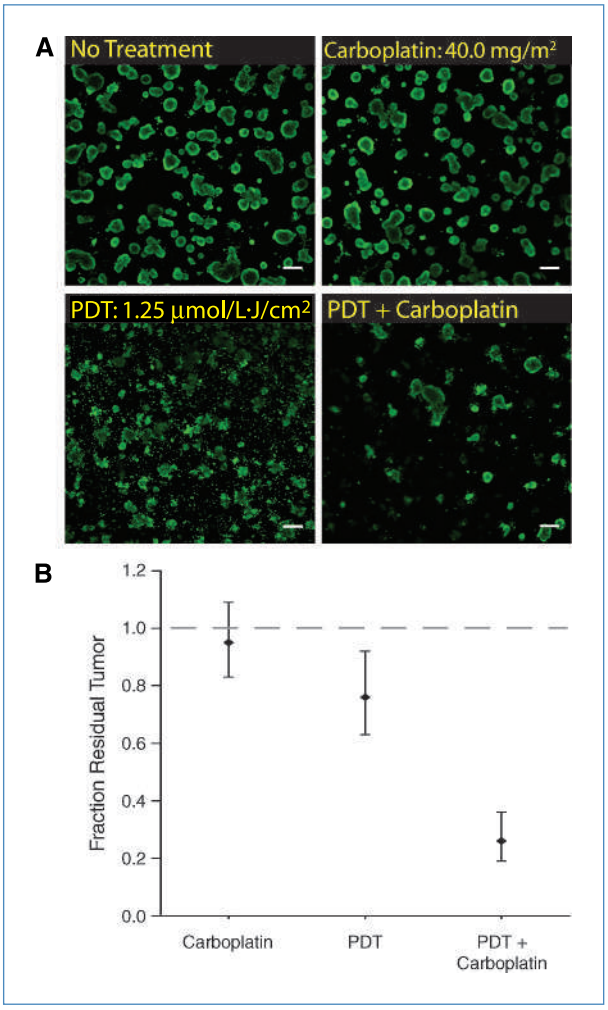

Figure 4. BPD-PDT synergizes with low-dose carboplatin to reduce residual tumor volume. A, images of residual disease (calcein). B, fraction residual tumor following carboplatin alone or BPD-PDT alone was 0.95 (95% CI, 0.83–1.09; n = 11) and 0.76 (95% CI, 0.63–0.92; n = 15), respectively, relative to no treatment (gray dashed line). The combination treatment, BPD-PDT followed by carboplatin, produced a synergistic reduction in residual tumor to 0.26 (95% CI, 0.19–0.36; n = 11; $P < 0.0001$, interaction term from ANCOVA). Scale bars, 250 µm.

micronodules with low-dose carboplatin (40 mg/m^2) either before or after 1.25 µmol/L·J/cm^2 BPD-PDT to determine the effect of treatment order.

Treatment with BPD-PDT prior to carboplatin produced a significant synergistic reduction ($P < 0.0001$, interaction term from ANCOVA) in residual tumor volume and viability compared with the monotherapies, relative to no treatment (n = 14). Mean fraction residual tumor in the combination treatment group was 0.26 (95% CI, 0.19–0.36; n = 11) compared with 0.76 (95% CI, 0.63–0.92; n = 15) with PDT alone and 0.95 (95% CI, 0.83–1.09; n = 11) with carboplatin alone (Fig. 4). Mean fraction viability in the combination PDT + carboplatin–treated group was 0.45 (95% CI, 0.38–0.53; n = 11) compared with PDT alone (0.80; 95% CI, 0.74–0.86; n = 15) or carboplatin alone (0.92; 95% CI, 0.88–0.97; n = 11; Fig. 5).

Conversely, no synergy was observed between the monotherapies with the reverse treatment order; carboplatin followed by BPD-PDT (Fig. 6). Mean fraction residual tumor burden with either PDT alone or carboplatin alone was 0.61 (95% CI, 0.55–0.68; n = 18) and 0.64 (95% CI, 0.61–0.67; n = 18), respectively, relative to no treatment (n = 18; Fig. 6A). The discrepancy in treatment response in the carboplatin-only arm between the two sequences (Figs. 4 and 6A or Figs. 5 and 6B), is due to the adjustment in the time point of evaluation necessitated by a fixed carboplatin schedule and duration as described in Materials and Methods. Compared with the monotherapies, the reverse combination treatment produced the most substantial decrease in mean fraction residual tumor burden (0.36; 95% CI, 0.34–0.39; n = 18), but this reduction was not synergistic (P = 0.3326, ANCOVA). Similarly, mean fraction viability in micronodules treated with either PDT alone or carboplatin alone was 0.78 (95% CI, 0.74–0.82; n = 18) and 0.79 (95% CI, 0.77–0.82; n = 18), respectively, compared with 0.65 (95% CI, 0.62–0.69; n = 18) in the combination carboplatin + PDT group, indicating no interaction between the two modalities (P = 0.1368, ANCOVA; Fig. 6B).

Discussion

PDT has shown clinical promise for the treatment of disseminated OvCa (14–17, 19) and will likely be most effective as part of a multifaceted treatment strategy to overcome resistance mechanisms that lead to treatment failure. The data presented in this study demonstrate a treatment order–dependent synergism with BPD-PDT and low-dose carboplatin using a 3D high-throughput reporter for adherent ovarian micrometastases.

Mechanistic differences between the individual modalities could account for the sequence-dependent synergism. Carboplatin is hydrolyzed as it enters a cell, creating an active species that forms interstrand and intrastrand DNA adducts. Depending on the extent of damage, the cell either enters cell cycle arrest or undergoes apoptosis, probably via ATM-CHK2–mediated activation of p53 in the nucleus (8, 43). This triggers transcriptional upregulation of proapoptotic proteins Bax/Bak and downregulation of antiapoptotic Bcl-2/Bcl-X_L in the cytosol, causing permeabilization of the outer mitochondrial membrane. Cytochrome c is subsequently released from the mitochondria followed by activation of caspase 9 and effector caspases 3, 6, and 7, which triggers the apoptotic machinery that is responsible for DNA fragmentation and protein degradation typical of programmed cell death (8, 23, 42, 43).

In contrast, BPD-PDT bypasses the nuclear signaling pathways that platinum agents rely on by damaging the mitochondrial membrane and initiating cytochrome c–mediated apoptosis or by directly destroying Bcl-2 associated with the mitochondria or endoplasmic reticulum (ER; refs. 4, 18, 26, 27, 29, 31). The observed synergism between the two modalities could, therefore, be explained by

a combination of three possible mechanisms. (*a*) BPD-PDT is in itself cytotoxic to target cells and decreases the size of residual ovarian tumors. As recently quantified by Celli and colleagues (37), BPD-PDT shifts OvCa size distribution toward smaller nodules, in contrast to carboplatin, which had minimal effect on size reduction. These results could have important implications for designing more effective therapeutic regimens, because small OvCa nodules are associated with significantly better PFS, OS, and response to chemotherapy than large tumors (5, 42). (*b*) BPD-PDT also disrupts nodular architecture creating tumors that are more vulnerable to carboplatin. High cellular density is a critical barrier to the penetration and accumulation of chemotherapeutic agents in tumors (7). Treatment-induced apoptosis has specifically been shown to decrease cellular density and enhance the uptake of chemotherapies into tumor micronodules (7). Therefore, BPD-PDT–mediated apoptotic disruption of micronodular architecture could play an important role in improving the delivery of platinum-based agents into residual OvCa nodules. This enhanced diffusion is particularly important within the context of i.p. administration of carboplatin, which relies on surface penetration of the drug to achieve therapeutic benefit (42, 44). (*c*) At the subcellular level, BPD-PDT sensitizes surviving cells to nuclear apoptotic signaling initiated by carboplatin, thereby lowering the threshold required to achieve a cytotoxic effect. The sequence-dependent synergism could therefore be driven by the ability of BPD-PDT to reduce the size and disrupt the structure of ovarian micronodules, in addition to sensitizing the cells to apoptotic signals from carboplatin treatment. Additional studies are necessary to elucidate the mechanisms for the observed synergism and to cross validate these findings with tumor regrowth in 3D as well as focused *in vivo* and patient tissue experiments.

The applicability of these findings to a broader library of photosensitizers and chemotherapies needs to be considered within the context of cytotoxic mechanisms. PDT-induced cellular damage can trigger a combination of nonspecific necrosis, apoptosis, or autophagy (18, 21). The predominance of a particular cytotoxic pathway depends on a variety of factors including the photophysical properties and preferred localization (and relocalization) sites of a photosensitizer, the local microenvironment, the fluence rate, and the PDT dose, as well as compensatory survival mechanisms (18, 21, 24–29). BPD, mesochlorin, and aluminum (III) phthalocyanine tetrasulfonate chloride (AlPcS(4)) localize primarily to the mitochondria and are efficient inducers of apoptosis (24, 26, 27, 29). A more complex response is observed with photosensitizers that localize to the ER such as AlPcCl and 9-capronyloxytetrakis (methoxyethyl) porphycene (18). Depending on the PDT dose, autophagy can be induced as either a prosurvival or prodeath pathway, which could be important in cells with defective apoptotic machinery or resistance to apoptosis and should be considered in mechanism-based combination regimens.

A variety of photosensitizers have been studied for PDT-mediated potentiation of chemotherapeutic agents including Photofrin, Photofrin II, δ-aminolevulinic acid (5-ALA), mesochlorin e_6 monoethylene diamine (Mce_6), metatetra(hydroxyphenyl)chlorin (m-THPC; Foscan), and indocyanine green (ICG; ref. 21). The chemotherapeutic agents evaluated were cisplatin, doxorubicin, and mytomicin C, which mediate cell death via DNA adducts (21). PDT in combination with these pharmacologic therapies was shown to enhance tumor destruction and reduce toxicity compared with chemotherapy alone (21). The optimal treatment sequence, however, was dependent on the photosensitizer and chemotherapeutic agents that were used. Cisplatin cytotoxicity was enhanced most significantly when the chemotherapeutic was administered before Photofrin or ICG-based PDT. Similarly, the strongest potentiation of mitomycin C efficacy was seen

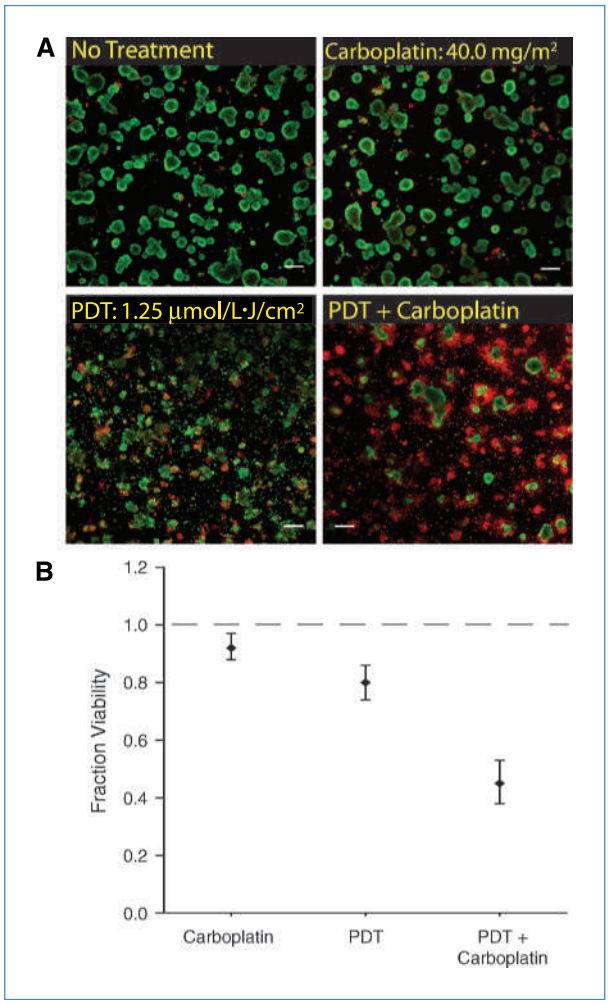

Figure 5. BPD-PDT followed by carboplatin synergistically reduces tumor viability. A, images of tumor viability (calcein and ethidium bromide fluorescence) following treatment. B, mean fraction viability in micronodules treated with either carboplatin alone or BPD-PDT alone was 0.92 (95% CI, 0.88–0.97; $n = 11$) and 0.80 (95%CI, 0.74–0.86; $n = 15$), respectively, relative to no treatment (gray dashed line). The combination treatment, BPD-PDT followed by carboplatin, reduced viability to 0.45 (95% CI, 0.38–0.53; $n = 11$), indicating a significant synergism ($P < 0.0001$, interaction term from ANCOVA). Scale bars, 250 μm.

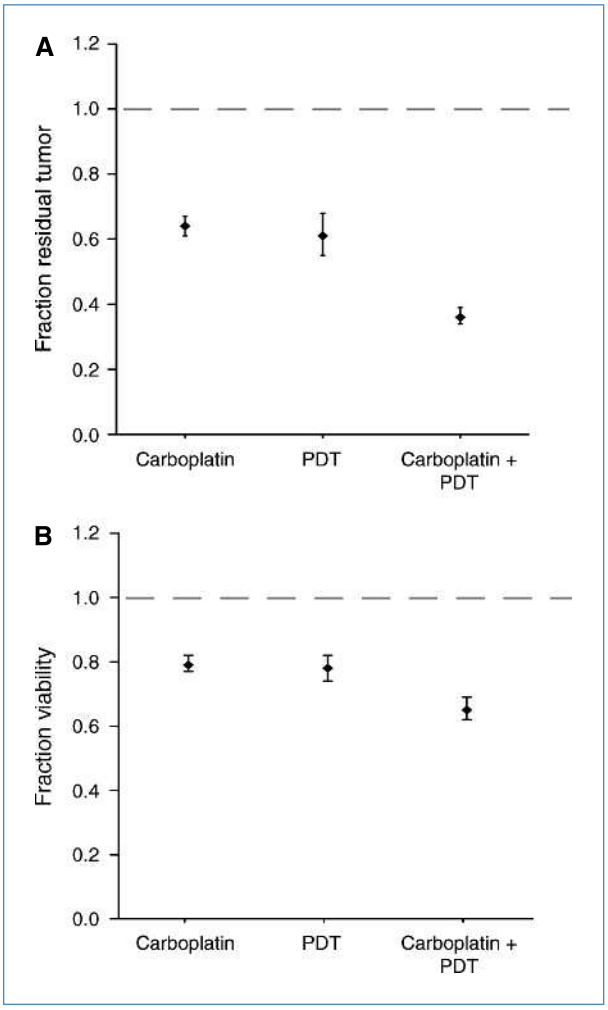

Figure 6. Carboplatin treatment prior to BPD-PDT does not produce a synergistic interaction. No synergism was observed with the reverse treatment order, as evaluated by fraction of residual tumor (A; $P = 0.3326$) and tumor viability (B; $P = 0.1368$; interaction term from ANCOVA for both treatment response metrics), relative to no treatment (gray dashed lines).

when the drug was delivered prior to Photofrin II or 5-ALA–mediated PDT. Conversely, doxorubicin was most effective after treatment with Photofrin II, Mce_6, or m-THPC–based PDT.

The *in vitro* 3D platform for micrometastatic OvCa described here fills a critical niche in translational science by bridging the gap between resource-intensive animal models and traditional monolayer cultures that lack important determinants of tumor growth and treatment response. Consistent with previous findings (12, 45), our results indicate that traditional monolayer cultures significantly overestimate the sensitivity of OvCa cells to cytotoxic treatments, which limits their value as tools to evaluate therapeutic efficacy. In contrast, tumor reduction in the same cells grown in 3D culture was comparable with results from *in vivo* studies (4, 31), which demonstrated that, as in the present study, multiple rounds of BPD-PDT or rationally designed combinations were necessary to achieve significant therapeutic benefit. An additional strength of the 3D platform is the demonstrated ability to evaluate dosing schedules over a time period that more closely mimics *in vivo* experiments than monolayer cultures. High-resolution longitudinal imaging of cytotoxicity in the 3D platform also reveals differential cytotoxic patterns for carboplatin and BPD-PDT on a nodule-by-nodule basis that would be impossible to uncover in monolayer. These capabilities, combined with a system for high-throughput screening, facilitate rapid optimization of treatment parameters and allow valuable resources for *in vivo* and patient tissue studies to be focused on the most promising regimens.

The treatment response factors addressed by this system include interaction of the monotherapies at the subcellular level and architectural disruption of ovarian nodules by BPD-PDT, suggesting improved delivery of carboplatin. Future models will incorporate more complex aspects of the tumor microenvironment including cocultures with stromal partners including fibroblasts and endothelial cells. These cocultures are motivated in part by clinical findings from Menon and colleagues (46), who showed that nodules as small as 1 mm (the smallest evaluated in the study) showed evidence of vascularity in peritoneal malignancies, including ovarian carcinomatosis. As the authors suggest, it was not clear if the vasculature in the smallest nodules was functional or even properly organized (46). It is important to explore whether endothelial cells, as signaling partners, have an effect on tumor growth or treatment response, even in the absence of flow or structural organization. New *in vitro* models for ovarian micrometastases using customizable matrices and stromal cells are being investigated by our group (47) and others (48, 49) and will play an increasingly important role in screening combination regimens and uncovering resistance mechanisms.

Within the context of designing effective multifaceted treatments for OvCa, PDT-based combination regimens have been shown to reverse cisplatin resistance (13), to synergistically increase the therapeutic effect of targeted biological therapies (4), and now to synergistically enhance carboplatin efficacy for the treatment of multifocal OvCa. These findings are particularly significant in view of the fact that the highly toxic therapies currently used to treat metastatic OvCa have produced only modest improvements in the recurrence rates and mortality associated with this disease.

In an effort to address this challenge of a narrow therapeutic window, we used doses of BPD-PDT and carboplatin in this study that were substantially lower than the typical range used *in vivo* and in the clinic (24, 34, 42, 44, 50). Keeping in mind the need for well-tolerated treatments, tumor destruction could be further improved with incremental and concomitant increases in the doses of both monotherapies. This approach will likely be more successful than significantly increasing either monotherapy to higher and more toxic levels. Also, in contrast to carboplatin (23, 42, 44), PDT can be administered in multiple rounds without additive host toxicity (4, 31). This attribute, along with the ability

of PDT to sensitize chemoresistant and chemosensitive OvCa nodules to platinum-based agents (13), highlights the need to explore the effect of repeatedly treating 3D micronodules with low-dose BPD-PDT in combination with low-dose carboplatin. The high throughput capabilities of the platform described here can be harnessed to evaluate these additional treatment scenarios and to inform focused preclinical experiments.

The results and strategies presented here could be used to design more effective and well-tolerated clinical combination regimens based on previously published studies using PDT to treat a variety of disseminated peritoneal malignancies, including ovarian carcinomatosis (14–19). Phases I and II PDT clinical trials using nonoptimized treatment parameters and Photofrin have shown promise in treating cytoreduced minimal residual disease and chemoresistant peritoneal tumors (17). Photofrin-PDT conferred a survival advantage relative to historical controls with acute but reversible toxicities. Furthermore, OvCas were among the most responsive intraabdominal solid tumors to i.p. PDT (17). Building on these promising findings, we predict that BPD-PDT (which offers significant pharmacokinetic and photobiological advantages over early generation photosensitizers; refs. 4, 29–31) in combination with low-dose carboplatin will be an effective and well-tolerated combination regimen.

Collectively, these preclinical and clinical reports indicate that PDT should be included in the regular armamentarium used to treat ovarian carcinomatoses as part of a comprehensive treatment plan designed to minimize toxicity with optimal cytoreductive effects. We envision a scenario in which BPD-PDT is used in conjunction with cytoreductive surgery to treat and sensitize unresectable tumors to chemo-, radio- and biological therapeutics. Due to the vast library of candidate interventions, high-throughput 3D treatment response platforms, as presented here, will play a critical role in selecting the appropriate combination regimens for multifocal OvCa as well as many other lethal metastatic cancers.

Disclosure of Potential Conflicts of Interest

No potential conflicts of interest were disclosed.

Grant Support

NIH grants RO1CA119388, RO1CA146337, and RO1AR040532 (T. Hasan); WCP Graduate Student Fellowship (I. Rizvi); MBRC Tosteson Fellowship; and National Cancer Institute grant F32CA138153 (C.L. Evans).

The costs of publication of this article were defrayed in part by the payment of page charges. This article must therefore be hereby marked *advertisement* in accordance with 18 U.S.C. Section 1734 solely to indicate this fact.

Received 05/27/2010; revised 08/13/2010; accepted 09/23/2010; published OnlineFirst 11/09/2010.

References

1. Bast RC, Jr., Hennessy B, Mills GB. The biology of ovarian cancer: new opportunities for translation. Nat Rev Cancer 2009;9:415–28.
2. Cho KR, Shih Ie M. Ovarian cancer. Annu Rev Pathol 2009;4: 287–313.
3. Naora H, Montell DJ. Ovarian cancer metastasis: integrating insights from disparate model organisms. Nat Rev Cancer 2005;5:355–66.
4. del Carmen MG, Rizvi I, Chang Y, et al. Synergism of epidermal growth factor receptor-targeted immunotherapy with photodynamic treatment of ovarian cancer *in vivo*. JNCI 2005;97:1516–24.
5. Chi DS, Eisenhauer EL, Zivanovic O, et al. Improved progression-free and overall survival in advanced ovarian cancer as a result of a change in surgical paradigm. Gynecol Oncol 2009;114:26–31.
6. Minchinton AI, Tannock IF. Drug penetration in solid tumours. Nat Rev Cancer 2006;6:583–92.
7. Au JL, Jang SH, Zheng J, et al. Determinants of drug delivery and transport to solid tumors. J Control Release 2001;74:31–46.
8. Agarwal R, Kaye SB. Ovarian cancer: strategies for overcoming resistance to chemotherapy. Nat Rev Cancer 2003;3:502–16.
9. Martin LP, Schilder RJ. Management of recurrent ovarian carcinoma: current status and future directions. Semin Oncol 2009;36:112–25.
10. Guarneri V, Piacentini F, Barbieri E, Conte PF. Achievements and unmet needs in the management of advanced ovarian cancer. Gynecol Oncol 2010;117:152–8.
11. Griffith LG, Swartz MA. Capturing complex 3D tissue physiology *in vitro*. Nat Rev Mol Cell Biol 2006;7:211–24.
12. Sharma SV, Haber DA, Settleman J. Cell line-based platforms to evaluate the therapeutic efficacy of candidate anticancer agents. Nat Rev Cancer 2010;10:241–53.
13. Duska LR, Hamblin MR, Miller JL, Hasan T. Combination photoimmunotherapy and cisplatin: effects on human ovarian cancer *ex vivo*. J Natl Cancer Inst 1999;91:1557–63.
14. Hahn SM, Fraker DL, Mick R, et al. A phase II trial of intraperitoneal photodynamic therapy for patients with peritoneal carcinomatosis and sarcomatosis. Clin Cancer Res 2006;12:2517.
15. DeLaney TF, Sindelar WF, Tochner Z, et al. Phase I study of debulking surgery and photodynamic therapy for disseminated intraperitoneal tumors. Int J Radiat Oncol Biol Phys 1993;25:445–57.
16. Sindelar WF, DeLaney TF, Tochner Z, et al. Technique of photodynamic therapy for disseminated intraperitoneal malignant neoplasms. Phase I study. Arch Surg 1991;126:318–24.
17. Hendren SK, Hahn SM, Spitz FR, et al. Phase II trial of debulking surgery and photodynamic therapy for disseminated intraperitoneal tumors. Ann Surg Oncol 2001;8:65–71.
18. Kessel D, Reiners JJ, Jr. Apoptosis and autophagy after mitochondrial or endoplasmic reticulum photodamage. Photochem Photobiol 2007;83:1024–8.
19. Wierrani F, Fiedler D, Grin W, et al. Clinical effect of meso-tetrahydroxyphenylchlorine based photodynamic therapy in recurrent carcinoma of the ovary: preliminary results. Br J Obstet Gynaecol 1997;104:376–8.
20. Gomer CJ, Ferrario A, Luna M, Rucker N, Wong S. Photodynamic therapy: combined modality approaches targeting the tumor microenvironment. Lasers Surg Med 2006;38:516–21.
21. Zuluaga MF, Lange N. Combination of photodynamic therapy with anti-cancer agents. Curr Med Chem 2008;15:1655–73.
22. Hongrapipat J, Kopeckova P, Liu J, Prakongpan S, Kopecek J. Combination chemotherapy and photodynamic therapy with fab' fragment targeted HPMA copolymer conjugates in human ovarian carcinoma cells. Mol Pharm 2008;5:696–709.
23. Markman M. Pharmaceutical management of ovarian cancer: current status. Drugs 2008;68:771–89.
24. Celli JP, Spring BQ, Rizvi I, et al. Imaging and photodynamic therapy: mechanisms, monitoring, and optimization. Chem Rev 2010;110: 2795–838.
25. Dougherty TJ, Gomer CJ, Henderson BW, et al. Photodynamic therapy. J Natl Cancer Inst 1998;90:889–905.
26. Hasan T, Ortel B, Solban N, Pogue B. Photodynamic therapy of cancer. In: Kufe DW, Bast RCJ, Hait WN, et al, editors. Cancer Medicine. 7th ed Hamilton (Ontario): B.C. Decker, Inc; 2006, p. 537–48.
27. Kessel D, Castelli M. Evidence that bcl-2 is the target of three

photosensitizers that induce a rapid apoptotic response. Photochem Photobiol 2001;74:318–22.
28. Wilson BC. Photodynamic therapy for cancer: principles. Can J Gastroenterol 2002;16:393–6.
29. Granville DJ, Jiang H, An MT, Levy JG, McManus BM, Hunt DW. Bcl-2 overexpression blocks caspase activation and downstream apoptotic events instigated by photodynamic therapy. Br J Cancer 1999;79:95–100.
30. Aveline B, Hasan T, Redmond RW. Photophysical and photosensitizing properties of benzoporphyrin derivative monoacid ring A (BPD-MA). Photochem Photobiol 1994;59:328–35.
31. Molpus KL, Kato D, Hamblin MR, Lilge L, Bamberg M, Hasan T. Intraperitoneal photodynamic therapy of human epithelial ovarian carcinomatosis in a xenograft murine model. Cancer Res 1996;56: 1075–82.
32. NIH RePORT Expenditures and Results (RePORTER). Enhancing direct tumor cell cytotoxicity by manipulating growth factor signaling. 2010 [cited 2010 March 17]; Available from: http://projectreporter.nih.gov/reporter.cfm (Project 5PO1CA087971-08: 0005).
33. Lurje G, Lenz HJ. EGFR signaling and drug discovery. Oncology 2009;77:400–10.
34. Lewis R, Schuman L, Mickler M, et al. Preclinical evaluation of cetuximab and benzoporphyrin derivative-mediated intraperitoneal photodynamic therapy in a canine model. 35th Meeting of the American Society for Photobiology. Brown University, Providence (RI): American Society for Photobiology; 2010, p. 34.
35. Petersen OW, Ronnov-Jessen L, Howlett AR, Bissell MJ. Interaction with basement membrane serves to rapidly distinguish growth and differentiation pattern of normal and malignant human breast epithelial cells. Proc Natl Acad Sci U S A 1992;89:9064–8.
36. Debnath J, Muthuswamy SK, Brugge JS. Morphogenesis and oncogenesis of MCF-10A mammary epithelial acini grown in three-dimensional basement membrane cultures. Methods 2003;30:256–68.
37. Celli JP, Rizvi I, Evans CL, Abu-Yousif AO, Hasan T. Quantitative imaging reveals heterogeneous growth dynamics and treatment-dependent residual tumor distributions in a three-dimensional ovarian cancer model. J Biomed Opt 2010;15:051603–10.
38. Evans CL, Rizvi I, Hasan T, de Boer JF. *In vitro* ovarian tumor growth and treatment response dynamics visualized with time-lapse OCT imaging. Opt Express 2009;17:8892–906.
39. Sundfeldt K. Cell-cell adhesion in the normal ovary and ovarian tumors of epithelial origin; an exception to the rule. Mol Cell Endocrinol 2003;202:89–96.
40. Demeter A, Sziller I, Csapo Z, et al. Molecular prognostic markers in recurrent and in non-recurrent epithelial ovarian cancer. Anticancer Res 2005;25:2885–9.
41. Franke FE, Von Georgi R, Zygmunt M, Munstedt K. Association between fibronectin expression and prognosis in ovarian carcinoma. Anticancer Res 2003;23:4261–7.
42. Fujiwara K. Can carboplatin replace cisplatin for intraperitoneal use? Int J Gynecol Cancer 2008;18 Suppl 1:29–32.
43. Ashkenazi A. Targeting the extrinsic apoptosis pathway in cancer. Cytokine Growth Factor Rev 2008;19:325–31.
44. Markman M. Intraperitoneal chemotherapy in the management of ovarian cancer: focus on carboplatin. Ther Clin Risk Manag 2009; 5:161–8.
45. Ohmori T, Yang JL, Price JO, Arteaga CL. Blockade of tumor cell transforming growth factor-βs enhances cell cycle progression and sensitizes human breast carcinoma cells to cytotoxic chemotherapy. Exp Cell Res 1998;245:350–9.
46. Menon C, Kutney SN, Lehr SC, et al. Vascularity and uptake of photosensitizer in small human tumor nodules: implications for intraperitoneal photodynamic therapy. Clin Cancer Res 2001;7: 3904–11.
47. Abu-Yousif AO, Rizvi I, Evans CL, Celli JP, Hasan T. PuraMatrix encapsulation of cancer cells. Journal of Visualized Experiments 2009 December 17 [cited 2010 July]; Available from: http://www.jove.com/index/details.stp?ID=1692.
48. Kenny HA, Krausz T, Yamada SD, Lengyel E. Use of a novel 3D culture model to elucidate the role of mesothelial cells, fibroblasts and extra-cellular matrices on adhesion and invasion of ovarian cancer cells to the omentum. Int J Cancer 2007;121: 1463–72.
49. Burleson KM, Boente MP, Pambuccian SE, Skubitz AP. Disaggregation and invasion of ovarian carcinoma ascites spheroids. J Transl Med 2006;4:6.
50. Pereira SP. Photodynamic therapy for pancreatic and biliary tract carcinoma. Optical Methods for Tumor Treatment and Detection: Mechanisms and Techniques in Photodynamic Therapy XVIII; 2009; San Jose CA, USA: SPIE; 2009. p. 71640J-10.